Revisiting the BTGNX - Localization of Sound Sources in Tip-Gap Flow

Vladimir Lebedev[1], Jan W. Delfs[2], Philipp Dietrich[1], Andreas Lucius[1], Florian Lex[1]

[1] *ebm-papst Mulfingen GmbH & Co. KG, 74672 Mulfingen, E-Mail: vladimir.lebedev@de.ebmpapst.com*
[2] *DLR, Inst. für Aerodynamik und Strömungstechnik, 38106 Braunschweig,*

Abstract

At last year's DAGA results for the Brunswick Tip-Gap Noise-Experiment (BTGNX) were presented [1]. The aim of the BTGNX was to provide high-fidelity data for the flow and the resulting aeroacoustics in the gap between an airfoil and a flat plate, which represents e.g. the flow between an axial fan blade and the wall ring.

This work mainly focusses on the localization of sound sources in the tip-gap region. The sound source localization is performed with conventional beamforming algorithms. Additionally, the recently proposed localization using the diffraction filter is also shown and compared to the conventional approach [2].

Here the influence of the winglet geometry, which significantly affects the tip-gap flow and the resulting acoustics, will be highlighted. The localization is performed for four different winglet geometries in the reference configuration (u = 40 m/s, 10 mm tip-gap, AoA = 12°). The numerical data is provided by scale-resolved CFD simulations using the commercial software Star-CCM+.

Experimental Setup

Fig. 1 shows the experimental setup. In front of the wind tunnel jet a table with a mounted airfoil and an additional top-plate is installed. The airfoil can be rotated, which allows a variation of the angle of attack. It can also be traversed vertically, which allows a variation of the tip-gap size. Different winglet geometries were also investigated, see fig. 2.

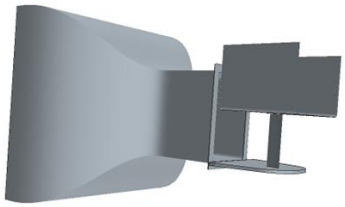

Figure 1: Sketch of experimental setup, wind tunnel jet on the left, table with mounted airfoil and top-plate on the right

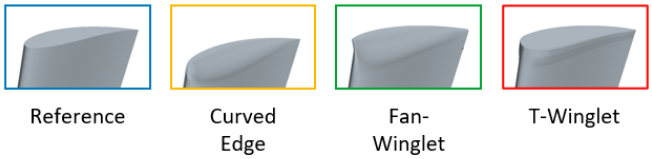

Figure 2: Overview of investigated winglet geometries

Methods

This investigation focuses solely on numerical data. For this scale-resolved CFD simulations using the commercial solver Siemens Star-CCM+ for the four different winglet geometries in the reference configuration (flow velocity 40 m/s, AoA 12°, 10 mm tip-gap) were carried out.

The sound source localization is performed with conventional beamforming (delay-and-sum). A 180-microphone spiral array on the suction side of the airfoil was used. The surface pressure fluctuations from the CFD simulation were propagated via FW-H to said array.

Additionally, the rather novel approach using the diffraction filter for the source localization is shown. This approach separates the large hydrodynamic pressure fluctuations, which do not propagate into the farfield, from the smaller acoustic fluctuations. The diffraction filter is defined by eq. 1, where $\boldsymbol{x}$ is the position of the receiver and $\boldsymbol{\xi}$ the position of the source and c is the sound of speed. The distance is defined as $\boldsymbol{r} = \boldsymbol{x} - \boldsymbol{\xi}$ or as unit distance vector $\boldsymbol{e_r} = \frac{\boldsymbol{r}}{|\boldsymbol{r}|} = \frac{\boldsymbol{r}}{r}$. The surface normal is defined by $\boldsymbol{n}$ and p' is the fluctuating pressure calculated in the CFD simulation. This integral is to be seen as the Cauchy principal value (evaluation without $\boldsymbol{\xi} = \boldsymbol{x}$) and to be evaluated at the source time ($\tau = t - \frac{r}{c}$). The calculated quantity p_s qualifies for sound source localization.

$$p_s'(\boldsymbol{x}, t) = \frac{1}{4\pi} \int_{\partial V_B} \frac{\boldsymbol{e_r} \cdot \boldsymbol{n}}{cr} \frac{\partial p'}{\partial \tau} + \frac{\boldsymbol{e_r} \cdot \boldsymbol{n}}{r^2} p' dS(\boldsymbol{\xi}, \tau) \qquad (1)$$

Results

In fig. 3 the sound power level for the four different configurations is shown. The sound power level was calculated by propagation of the surface pressure fluctuations via FW-H to 1000 microphones distributed on a sphere with a radius of 2 meters around the airfoil. Then the microphone signals were averaged and frequency filtered. To account the sphere surface, the level was corrected by +17 dB.

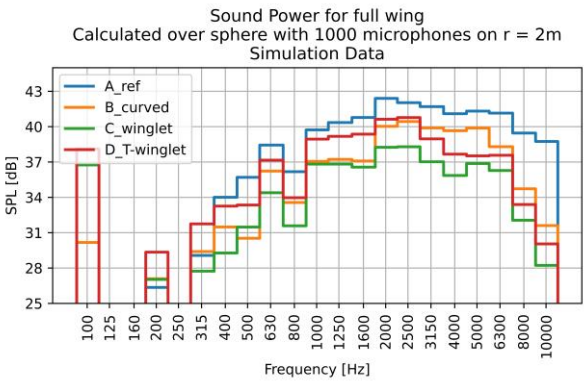

Figure 3: Comparison of sound power level over third-octave-frequency bands for different winglet configurations (blue: Reference, orange: Curved Edge, green: Fan-Winglet, red: T-Winglet)

For the further analysis three frequency bands were chosen: First the 1000 Hz band, where the winglets cluster in two groups: Reference and T-Winglet being 2 dB above the other

two. The 2000 Hz band shows the Reference 2 dB above the Curved Edge and the T-Winglet, which are again 3 dB above the Fan-Winglet. Finally, the 4000Hz band, where all configurations are separated.

Considering the 1000 Hz band, the beamforming results show a sound source in the rear tip-gap region for the worse performing winglets, see fig. 4. The localization via the diffraction filter is in good agreement, see fig. 5. The increased dynamic (40 dB, compared to 5 dB for beamforming) and spatial (not bound by wavelength) resolution shows additional sound sources at the bottom end of the airfoil and at the trailing edge for all the configurations. The sound sources in the tip-gap of the Reference configuration can be divided into two separate sources, the dominant source at the rear part/suction side edge and another secondary source at the front part/pressure side edge.

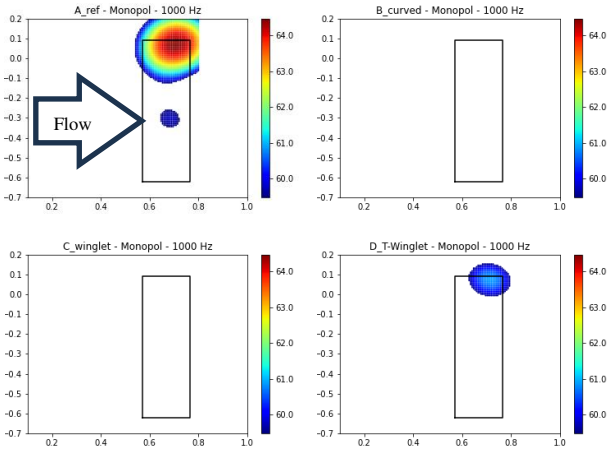

Figure 4: Sound maps for 1000 Hz band, calculated via conventional beamforming for different winglet geometries, upper left: Reference, upper right: Curved Edge, lower left: Fan-Winglet, lower right: T-Winglet

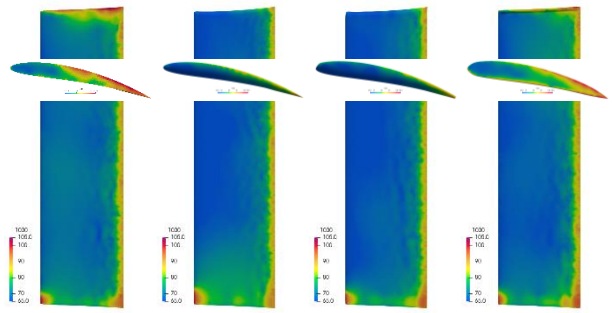

Figure 5: Sound maps for 1000 Hz band, calculated via the diffraction filter for different winglet geometries, in the background: view on the pressure side, additional view on the top of the wing in the foreground, from left to right: Reference, Curved Edge, Fan-Winglet, T-Winglet

Looking at the comparable sound power level for the 2000 Hz band for the Curved Edge and the T-Winglet one might assume the source situation being comparable. However, the source maps reveal completely different sources for both cases, see fig.6 and fig. 7. For the Curved Edge configuration, a source is found at the bottom-plate. However, the dominant source for the T-Winglet still sits at the rear of the tip-gap. This source at the bottom-plate is exclusive to the Curved Edge configuration. Because the configurations differ geometrically only at the upper end, this leads to two possible scenarios. The first assumes the sound source to be physical. This would imply that the winglet geometry strongly influences the (upstream and distant) flow field at the bottom plate. The other possibility is that the source is caused by underlying differences in the meshes used for the CFD simulation. Although the settings for the meshing were equivalent for all configurations, the automized workflow of the mesher of Star-CCM+ might lead to significant differences in the mesh. Further investigation of this sound source was not part of this work. In conclusion, this disparity emphasizes two key takeaways: First, a similar sound power level might be caused by two completely different effects and second, the careful interpretation of highly automized CFD results.

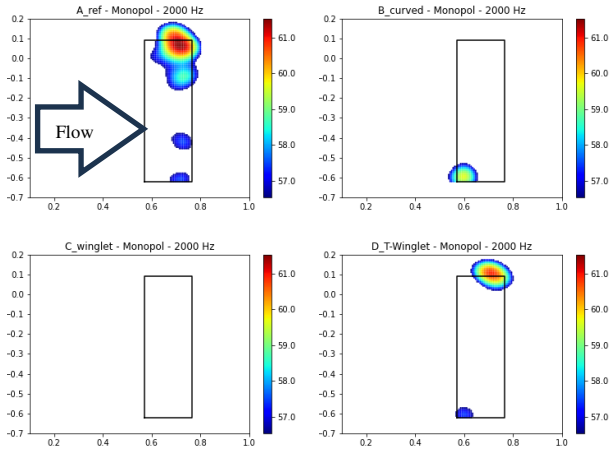

Figure 6: Sound maps for 2000 Hz band, calculated via conventional beamforming for different winglet geometries, upper left: Reference, upper right: Curved Edge, lower left: Fan-Winglet, lower right: T-Winglet

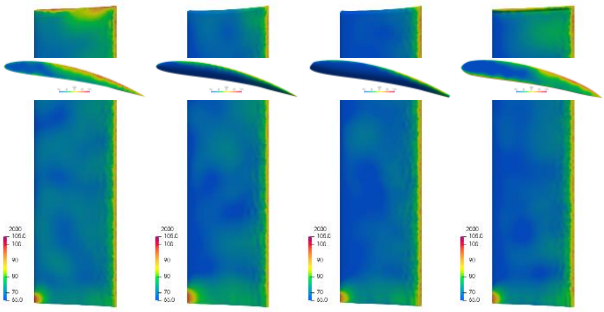

Figure 7: Sound maps for 2000 Hz band, calculated via the diffraction filter for different winglet geometries, in the background: view on the pressure side, additional view on the top of the wing in the foreground, from left to right: Reference, Curved Edge, Fan-Winglet, T-Winglet

The sound maps for the 4000 Hz band show different source regions for all four configurations, see fig. 8 and fig. 9. The beamforming maps show the most dominant source for the Curved Edge configuration, which is at the middle of the tip-gap. This is in contradiction with the sound power level for the 4000 Hz band, where the Reference configuration is 2 dB above the Curved Edge. This might be caused by the use of a planar array or rather the directivity of the source. Also, for the Reference case, the two source localization methods are

not in agreement. The dominant source for the beamforming maps is at the front of the wing, while the diffraction filter highlights the rear part as the dominant one.

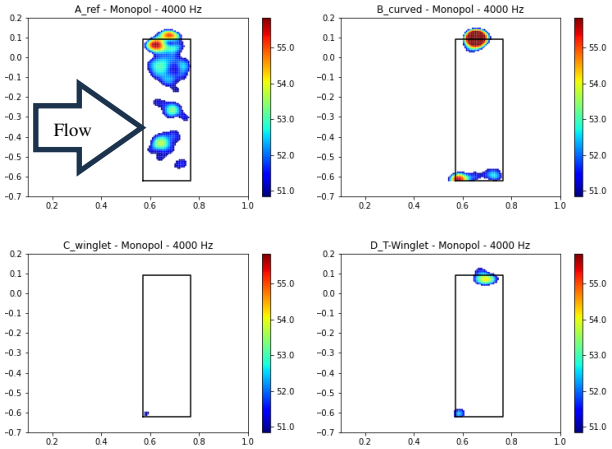

Figure 8: Sound maps for 4000 Hz band, calculated via conventional beamforming for different winglet geometries, upper left: Reference, upper right: Curved Edge, lower left: Fan-Winglet, lower right: T-Winglet

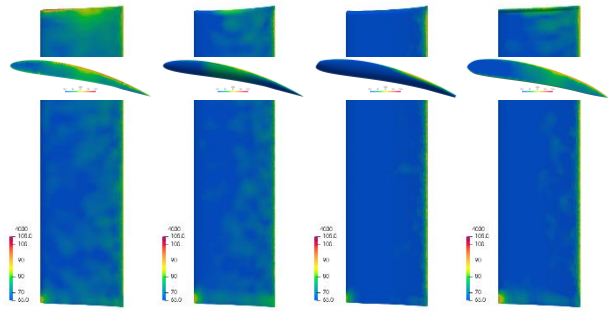

Figure 9: Sound maps for 4000 Hz band, calculated via the diffraction filter for different winglet geometries, in the background: view on the pressure side, additional view on the top of the wing in the foreground, from left to right: Reference, Curved Edge, Fan-Winglet, T-Winglet

Conclusion

For most geometries and frequencies, the sound source localization via beamforming and via the diffraction filter is in good agreement.

Based on the sound sources, the winglets can be clustered in two groups: First, the Reference and T-Winglet, which showed dominant sources in the tip-gap region throughout all frequencies. In most cases the source was at the rear tip-gap, closer to the suction side edge. The second cluster consists of the Curved Edge and the Fan-Winglet. These configurations showed no sources (except for 4 kHz for Curved Edge) in the tip-gap. This shows that the rounding of the pressure side edge leads to the largest decrease in sound sources and respectively emitted noise.

Because all these sound sources are flow induced and to explain the effect of the different geometries on the tip-gap flow, streamlines in the tip-gap region for the different winglet geometries are shown. Fig. 10 shows the flow around the Reference winglet. Two separate vortices can be identified, one rolling up over the pressure side edge at the front of the wing and another at the rear of the wing. Both positions were also identified as source locations, with the rear one being the dominant source. The tip-gap vortex interacts with the flow from the pressure side and the pressure side edge and leads to large sound generation. While the vortex at the front of the wing is also well formed, the sound source is only secondary. The flow around the T-Winglet, see fig. 11, shows a similar behavior, although both vortices are much smaller.

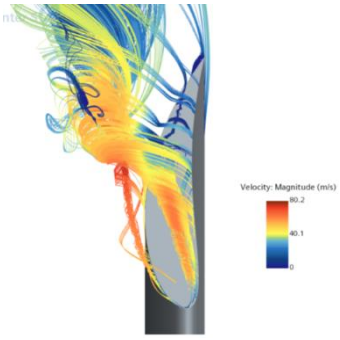

Figure 10: Streamlines around the Reference winglet, colorized with magnitude of velocity

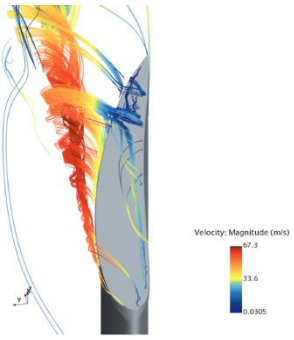

Figure 11: Streamlines around the T-Winglet, colorized with magnitude of velocity

In contrast, the Curved Edge and Fan-Winglet configurations lead to a much smaller tip-gap vortex, see fig. 12 and fig. 13. More importantly, the higher velocity flow through the tip-gap washes the vortex further from the airfoil away, which reduces the interaction with the suction side edge and the emitted sound. The flow fields show no clear difference at around 50% chord, which could be attributed to the additional sound source in the tip-gap at 4000 Hz for the Curved Edge configuration.

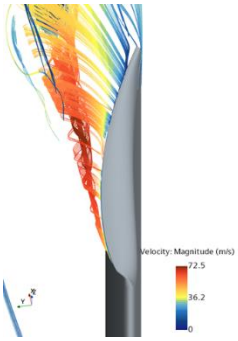

Figure 12: Streamlines around the Fan-Winglet, colorized with magnitude of velocity

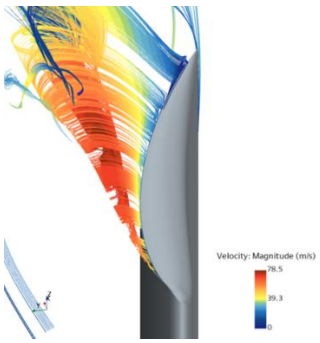

Figure 13: Streamlines around the Curved Edge winglet, colorized with magnitude of velocity

Literature

[1] Reuschling, F., Liberson, L., Ernst, D., Pott-Pollenske, S. M., & Delfs, J. W. (2024). BTGNX: Windkanalexperiment zu kopfspaltströmungsinduzierter Geräuschentstehung-Teil 2: Experimentelle Untersuchung. DAGA 2024.

[2] Delfs, J. W., Ruck, R., & Lebedev, V. (2024). Ermittlung von aerodynamischen Schallquellen auf turbulent überströmten Oberflächen. DAGA 2024.